Kerbala Journal of Pharmaceutical Sciences

ISSN: 2221-7207(Print) / **ISSN**: 3006-7189 (Online)

Effect of Modified Nanoparticles on the Levels of Some Important Proteins in Blood

Nada Y. Fairooz[1, *], Assel A. Hadi[2], Hussein K. Al-Hakeim[3]

[1]Department of Chemistry, Faculty of Science, Babylon University, Iraq

[2]Department of Biochemistry, College of Science, Al-Mustaqbal University, Iraq

[3]Department of Chemistry, Faculty of Science, Kufa University, Iraq

***Corresponding Author:**

Nada Y. Fairooz: fairoz.nada@yahoo.com

Received: 30/09/2025
Accepted: 27/11/2025
Published: 31/12/2025

Keywords: Manganese dioxide nanoparticles, protein adsorption, FSH, LH, nanocomposites.

DOI: 10.62472/kjps.v16.i27.241-258

Abstract

Manganese dioxide nanoparticles (MnO_2-NPs) and graphene oxide–based nanocomposites have attracted increasing attention for protein recovery applications. In this study, follicle-stimulating hormone (FSH) and luteinizing hormone (LH) were investigated as model glycoproteins for adsorption onto chitosan-coated MnO_2 nanoparticles (MnO_2-NPs) and chitosan/graphene oxide–MnO_2 nanocomposites (CS/GO-MnO_2-NPs). The CS/GO-MnO_2 nanocomposite was synthesized using a co-precipitation method and characterized by SEM, EDS, FT-IR, XRD, and particle size analysis. Adsorption experiments were conducted using fixed nanoparticle doses and varying hormone concentrations, and thermodynamic parameters were evaluated at different temperatures. The CS/GO-MnO_2-NPs exhibited high adsorption capacity for both hormones, following the Freundlich isotherm, indicating surface heterogeneity. Thermodynamic analysis confirmed that the adsorption process was spontaneous and exothermic. These findings suggest that MnO_2-based nanocomposites are promising platforms for hormone extraction and analytical applications involving human serum.

تأثير الجسيمات النانوية المُعدَّلة على مستويات بعض البروتينات المهمة في الدم

ندى فيروز، أسيل هادي، حسين الحاكم

الملخص

تتمتع جسيمات ثاني أكسيد المنغنيز النانوية (MnO_2-NPs) بإمكانات تطبيقية واسعة في العديد من المجالات، ويُعد استخدام المتراكبات النانوية لاسترجاع البروتينات القيّمة أحد الجوانب البارزة في هذا المجال البحثي. بهدف عزل بروتينات مفيدة من مصل الإنسان بشكل متزامن، استُخدم في هذه الدراسة هرمونا الغليكوبروتين: الهرمون المنبه للجريب (FSH) والهرمون اللوتيني (LH) كنماذج ممتزة، ليتم التقاطهما عبر الامتزاز التلقائي على جسيمات ثاني أكسيد المنغنيز النانوية المغلفة بالكيتوسان(MnO_2-NPs) ، وكذلك على سطح المتراكبات النانوية المعتمدة على أكسيد الغرافين.(CS/GO-MnO_2-NPs) تبحث هذه الدراسة في خصائص امتزاز هرموني FSH وLH، مع استخدام طريقة الترسيب المشترك لتحضير المتراكب النانوي .CS/GO-MnO_2 وقد جرى توصيف المواد المحضّرة باستخدام تقنيات تحليلية متعددة، شملت مطيافية تشتت الطاقة(EDS) ، والمجهر الإلكتروني الماسح(SEM) ، ومطيافية الأشعة تحت الحمراء بتحويل فورييه(FT-IR) ، وحيود الأشعة السينية(XRD) ، وتحليل حجم الجسيمات.(PSA) حُضنت محاليل الهرمونات بتراكيز مختلفة مع كميات ثابتة من الجسيمات النانوية لدراسة السعة النهائية للامتزاز، كما حُسبت المعلمات الثرموديناميكية لعملية الامتزاز بإجراء التجارب عند درجات حرارة مختلفة. وتشير نتائج الدراسة إلى أن قابلية هرموني FSH و LHعلى الامتزاز التلقائي على أسطح المتراكبات النانوية المعتمدة على أكسيد الغرافين (CS/GO-MnO_2-NPs) وجسيمات ثاني أكسيد المنغنيز النانوية المغلفة بالكيتوسان (MnO_2-NPs) قد تسهم في استخلاص البروتينات المفيدة من مصل الإنسان. يركز هذا العمل بشكل أساسي على تحليل امتزاز هرموني FSH وLH، مع توصيف المتراكب النانوي المُحضّر باستخدام تقنيات XRD و FT-IRو SEMو EDSو .PSAوقد أظهرت النتائج أن المتراكبات-CS/GO MnO_2-NPsتمتلك قدرة عالية على امتزاز الهرمونات، وأن عملية الامتزاز تتبع متساوي الامتزاز من نوع فريندلخ، مما يدل على عدم تجانس سطح المتراكب النانوي. كما أكدت الدراسات الثرموديناميكية أن آلية الامتزاز تلقائية وطاردة للحرارة.ولغرض تحديد قوى التفاعل بين جزيئات البرولاكتين (PRL) والأسطح، أُجريت اختبارات إزالة الامتزاز، بالإضافة إلى اختبار ELISA لتقييم مستوى .PRL وتُظهر نتائج هذا البحث أن امتزاز هرموني FSHو LHعلى أسطح جسيمات MnO_2-NPs يرتبط ببنية البروتين، ويجب أخذ هذه النتائج بنظر الاعتبار عند استخدام الجسيمات النانوية كوسط داعم لهذه الهرمونات في الأطقم التحليلية أو في عمليات استخلاص الهرمونات من المصل.

1. Introduction

Manganese dioxide (MnO2) is a cheap and naturally existing possible green oxide, which exhibits unusual some of its remarkable physical and chemical behaviours at room temperature (Fahdil A, AL-Niaimi D, 2018). There are numerous uses for this oxide in microwave absorbers, molecular adsorption, and ion exchange, biosensors and energy storage due to its rich polymorphism and structural diversity (Yano et al., 2022). Analysis of unusual optical, magnetic, mechanical and electrical properties of nanoscale morphologies has attracted a lot of attention over the recent years. Hormones can be inhibited through covalent bonding and physical adsorption onto Co-precipitation method-synthesized manganese dioxide nanoparticles. It is regarded as one of the safest methods to lower protein uptake. One of the advantages of co-precipitation is the ease with which the final particle size and content can be controlled, the particle surface state and overall homogeneity modified, and the preparative process accelerated [MW1]. Appropriate characterization techniques are required after CS/GO-MnO_2 NPs are synthesized in order to investigate the physico-chemical properties of the particles. We have used the Fourier transform infrared (FTIR), powder X-ray diffraction (XRD), scanning electron microscopy (SEM), and energy dispersive X-ray spectroscopy (EDS) techniques to analyze CS/GO-MnO_2 NPs for the purposes of such characterization. Characterizing the synthesized nanoparticles through the previously mentioned techniques is crucial to confirm their safety, effectiveness, and consistency for use in healthcare applications (Nugroho et al., 2023; Petrov et al., 2005; Yano et al., 2022).

2. Materials and Method

2.1 Synthesis of Manganese Dioxide Nps

All chemical reagents utilized were of analytical grade and handled according to the manufacturers' guidelines. To synthesize MnO_2, a standard preparation procedure was followed in which 0.18 g of $MnCl_2 \cdot 4H_2O$ was mixed with 50 mL of isopropanol in a round-bottom flask equipped with a reflux condenser. Under continuous stirring, this mixture was heated to around 83°C. Then, a hot solution containing 0.10 g of $KMnO_4$ dissolved in 5 mL of deionized (DI) water was added within seconds to the boiling solution to produce a thick black precipitate. The mixture was cooled to RT after 10 min, and then the precipitate was separated by centrifugation, washed several times with DI water, and finally dried overnight at 60 °C.

2.2 Synthesis of CS/GO-Mno_2 Nps

In order to manufacture graphene oxide, 500 milliliters of deionized (DI) water was used to dissolve a solution that contained 0.5 grams of graphene oxide and 0.1 grams of chitosan (CS) respectively (Sigma–Aldrich, USA). The mixture was then stirred at room temperature for two hours with 0.5 g of nanoparticles added. The supernatant was vortexed and centrifuged, followed by washing with DI water to remove unbound material, and then placed in an oven overnight at 80 °C to evaporate excess water to obtain the composite of the CS/GO-NPs.

2.3 Characterization of CS/GO-Mno_2 Nps

2.3.1 Scanning Electron Microscopy (SEM)

Materials and methods2.1. Preparation and characterization of CS/GO-MnO_2 nanoparticlesThe scanning electron microscope (SEM) was conducted on CS/GO-MnO_2 nanoparticles with an AIS2300C (AIS2300C, Korea) for analyzing the surface morphology and structural features. A thin gold layer was

deposited on top of the sample, the later with 1 mg placed on the SEM holder, in order to increase the current in the image and achieve a better image resolution before imaging.

2.3.2 X-Ray Diffraction (XRD)

X-ray diffraction (XRD) analysis of synthesized MnO_2 nanoparticles in 2θ from 10° to 100° (diffractometer with Cu Kα radiation ($\lambda = 0.15425$ nm)). The samples received were characterized by a diffractometer Shimadzu XR-6000, copper target, 40 kV, 30 mA. Using the Debye–Scherrer equation, the average crystallite size of the CS/GO-MnO_2 nanoparticles was determined as follow:

$D = k\lambda/((\beta \cos \theta))$ (where k (0.9) is the diffraction angle, θ is the X-ray wavelength, β is the full width at half maximum (FWHM) of the (370) diffraction peak, and) is the Scherrer constant.

2.3.3 Fourier Transform Infrared Spectrophotometer (FTIR)

Fourier-transform infrared (FTIR) spectra were obtained using a SHIMADZU FTIR 8400S spectrophotometer. The CS/GO-MnO_2 nanoparticles were blended with potassium bromide (KBr) to form a pellet, and the spectral data were recorded within the wavenumber range of 400–4000 cm^{-1}.

2.3.4 Particle Size Analysis (PSA)

Evaluation of the particle size distribution of the formed CS/GO-MnO_2 nanoparticles was performed via dynamic light scattering (DLS) using 90 Plus Particle Size Analyzer with 12 mm cell. Sample preparation was performed by dispersing a small amount of nanoparticle powder in pure methanol and sonicating for 10 min. The measurements were taken at 25°C and the physical parameters (density, refractive index, dielectric constant etc.) were adapted based on the CS/GO-MnO_2 nanoparticles and the dispersant. The pH of each suspension was adjusted to 7 and 10 with either NaOH or HCl, and their respective particle size distributions are shown in histogram format.

2.3.5 Zeta Potential Measurements

Using the 90 Plus Particle Size Analyzer, the electrophoretic mobility of CS/GO-MnO_2 nanoparticles was studied in order to investigate their zeta potential. Using electrophoretic mobility measurements and the Helmholtz–Smoluchowski equation, the zeta potential was calculated. 0.1 g of CS/GO-MnO_2 NPs were dispersed in 10 mL of methanol, sonicated for five minutes, and then measured at 25 °C to create the sample.

2.4 Interaction of Hormone FSH, and LH with CS/GO-MnO_2 NPs

To assess the interaction between FSH and LH hormones and CS/GO-MnO_2 nanoparticles, Eppendorf tubes containing different concentrations of CS/GO-MnO_2 NPs (5, 10, 15, 20, 25, 30, 35, and 40 mIU/mL) were each combined with 100 µL of the hormone solution. Hormone concentrations were converted to ng/mL in accordance with WHO guidelines. The mixtures were agitated for one hour, exceeding the equilibrium time reported in previous studies, and subsequently centrifuged at 4000 rpm for 20 minutes. The Enzyme-Linked Immunosorbent Assay (ELISA) kits (Monobind Co., USA) were used to evaluate the hormone levels in the resultant supernatant. The equation was used to determine how much hormone was absorbed onto the nanoparticles: $Q_e = X / m = [V(C_o - C_e)] / m$ where X represents V is the volume of the solution (mL), C_e is the equilibrium hormone concentration (ng/mL), m is the weight of the adsorbent, and ng is the amount of adsorbed hormone.

The relationship between Q_e and C_e is presented in the corresponding graphs. Equilibrium concentrations (C_e) were plotted to generate adsorption isotherms, enabling analysis and interpretation of the adsorption behavior. The Freundlich isotherm was found to best describe hormone adsorption onto CS/GO-MnO_2 nanoparticles and can be expressed linearly as:

log Q_e = log Kf + (1/n) log C_e Here, Kf, which depends on temperature and adsorption energy, reflects the adsorption capacity of the nanoparticles and helps evaluate the interaction process. The empirical constant *n* indicates the adsorption intensity, representing the strength of the driving force for adsorption. Additionally, human serum was used as an alternative source of hormones, and the adsorption experiments were repeated under the same conditions.

2.5 Thermodynamics of the Adsorption Process

Three distinct temperatures (298, 308, and 318 K) were used for the adsorption tests in order to calculate the adsorption process's thermodynamic parameters, ΔH°, ΔG°, and ΔS°. The equilibrium constant (K) and the adsorption isotherm at each temperature are obtained by subtracting the quantity of hormone (Q) in solution from the quantity adsorbed onto the CS/GO-MnO2-NPs surface. The weight of CS/GO-MnO2-NPs used in this uptake was4was as 0.02g (where Keq = 0.02Qe/0.1Ce represents the weight of CS/GO-MnO2-NPswas and Qe is the amount of hormone adsorbed). T: absolute temperature; R: gas constant (8.314 J. mol-1. K-1), the formula ΔG° = -RTlnKeq can be used to find the change in free energy, or ΔG°. The Van't Hoff equation (lnKeq = -ΔH°/RT + Constant) was used to determine the heat of adsorption (ΔH°). Plotting the suitable Ce versus the ln Keq for each concentration allowed for the identification of the equilibrium constant, Keq, which can be determined at a temperature where Ce approaches zero. The enthalpy of the adsorption process (ΔH°) can be found by When (InKeq) is plotted versus (1/T), a linear graph with a gradient of -ΔH°/R (Al-Hakeim et al., 2014). The formula ΔG° = ΔH° - TΔS° was used to determine the entropy change (ΔS°).

2.6. Desorption Process

To obtain the information on the amount of hormone desorbed from CS/GO-MnO2 NPs surface, desorption tests were performed. Since the amount desorbed often decreases with increasing desorption pressures, the cleavage of the adsorbate–adsorbent interaction is facile. According to the desorption statistics, FSH accounts for 61.97% of the total desorption. In order to draw more reliable conclusions about the nature of Table II displays the interactions between the adsorbent and adsorbate as well as the Freundlich constants for the hormone-CS/GO-MnO2 NPs combination. The intensity of adsorption is represented by a parameter n, which is used to identify the value at which maximum adsorption occurs and enables prediction of hormone release from the hormone–CS/GO-MnO_2nanoparticle system.

3-Results and Discussion

3.1 Adsorption Process

At 25°C, the maximum amount of FSH and LH hormones adsorbed onto the surface of CS/GO-MnO_2 nanoparticles was 7.07 µg/g. These findings indicate that CS/GO-MnO_2 NPs can effectively adsorb these hormones even at relatively low concentrations. The adsorption isotherms for FSH and LH on the CS/GO-MnO_2 NP surface are presented in Fig.1A-B, while the linearized Freundlich plots for hormone adsorption are shown in Fig.2A-B. The Freundlich plots provide a means to quantify and analyze hormone adsorption on the nanoparticle surfaces.

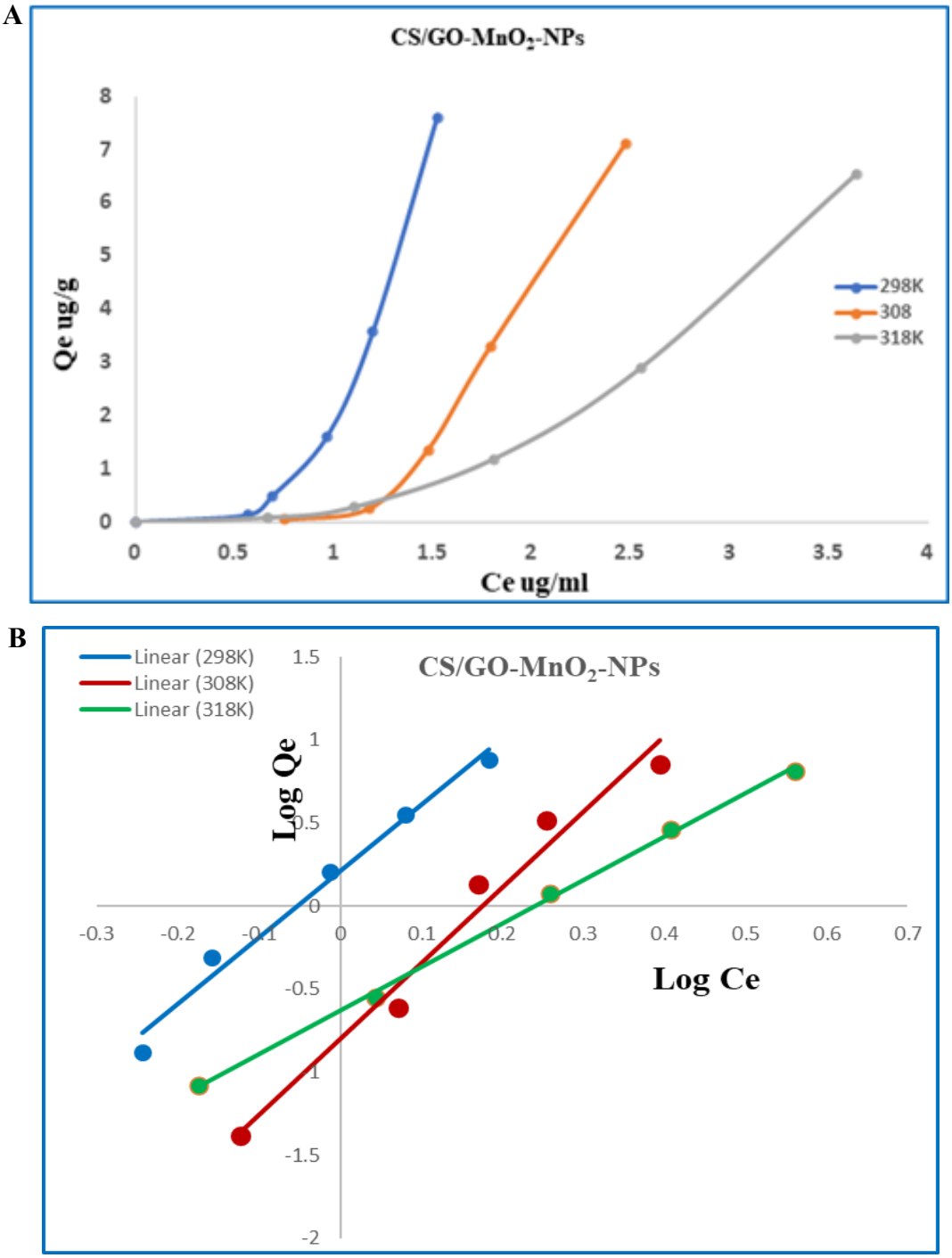

Figure1: Adsorption behavior of hormone/protein on CS/GO-MnO_2-NPs at different temperatures (298, 308, and 318 K). (A) Adsorption isotherms showing the relationship between equilibrium adsorption capacity (Qe) and equilibrium concentration (Ce). (B) Freundlich isotherm plots (log Qe versus log Ce), indicating heterogeneous surface adsorption and temperature-dependent adsorption behavior.

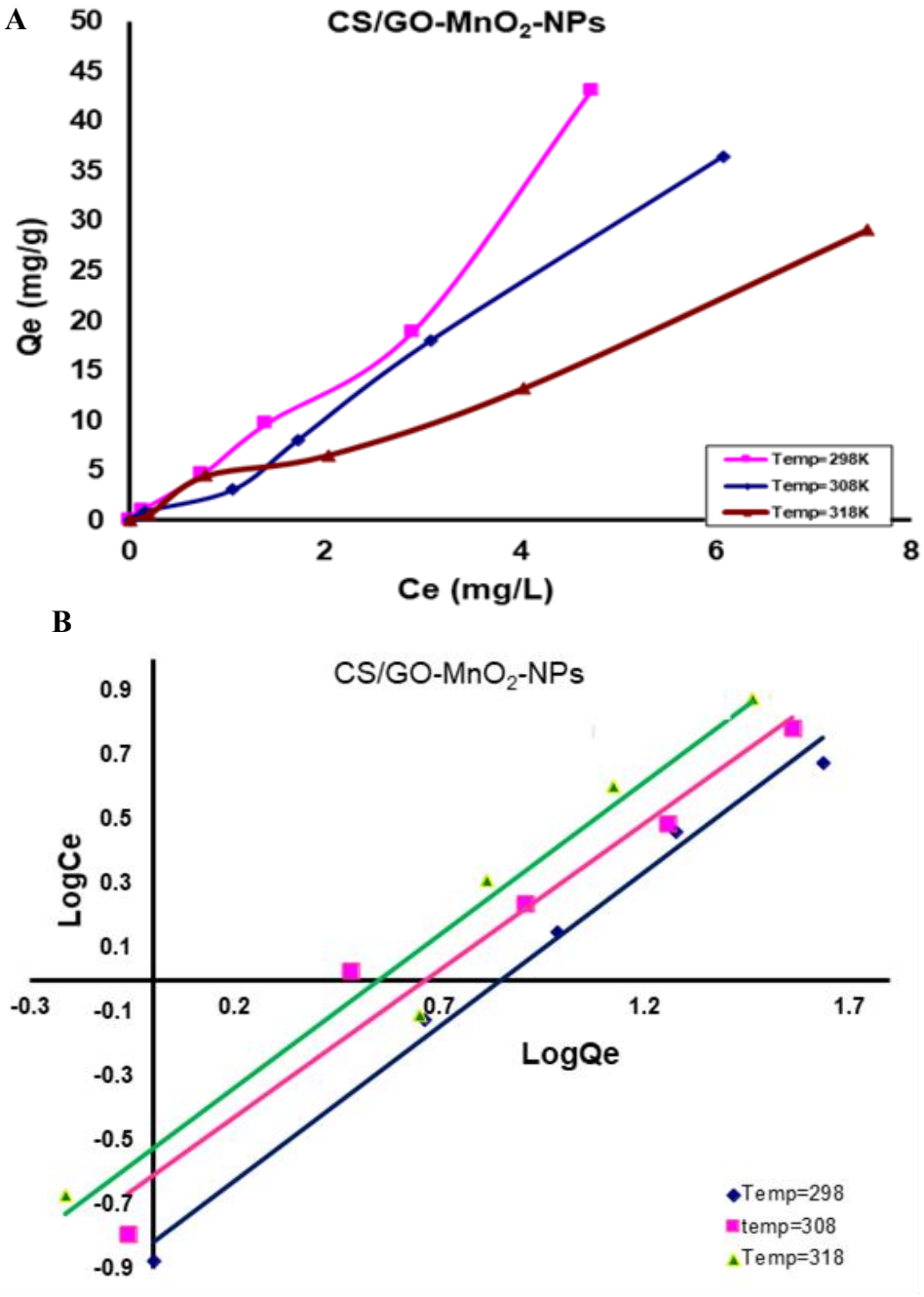

Figure2: Adsorption behavior of protein/hormone on CS/GO-MnO_2-NPs at different temperatures (298, 308, and 318 K). (A) Adsorption isotherms showing the relationship between equilibrium adsorption capacity (Qe) and equilibrium concentration (Ce). (B) Freundlich isotherm plots (log Qe versus log Ce), indicating heterogeneous surface adsorption and temperature-dependent adsorption characteristics.

3.2 Adsorption Process Thermodynamics

Fig.3 shows the Van't Hoff equation for the adsorption of FSH and LH hormones at near 298, 308, and 318 K at room temperature on the exterior ofCS/GO-MnO_2 NPs. The thermodynamic parameters for the hormone adsorption onto Table1 report the surface of the CS/GO-MnO2 NPs. Adsorption is an exothermic reaction that proceeds spontaneously.

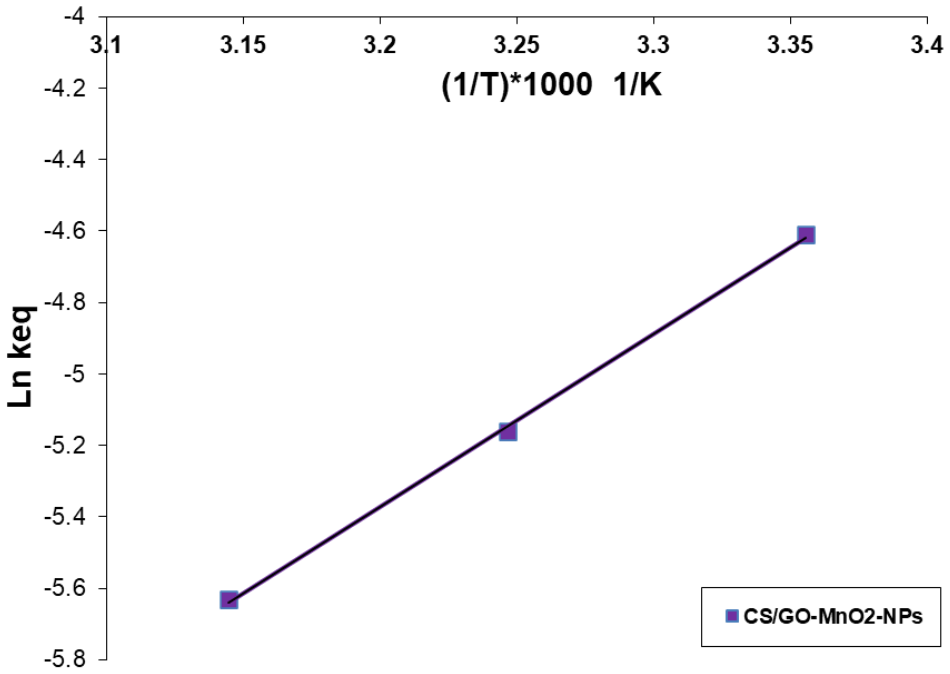

Figure3: An example of the Vant Hoff equation for the adsorption of FSH hormone on CS/GO-MnO_2 NP composite's surface

Table1: Physical and Chemical Characteristics of The Synthesized CS/GO-Mno_2 Nanoparticles

NPs	(1/T)*1000	$X_m = K_{eq}$	ln X_m	Gradient	ΔG°	ΔH°	ΔS°
CS/GO-MnO_2-NPs	3.356	0.00994	-4.611	4.362	11.425	-36.262	-160.021
	3.247	0.005736	-5.161				
	3.145	0.003584	-5.631				

The main discovery of the work is that CS/GO-MnO2 NPs' surface allows for the spontaneous adsorption of FSH and LH hormones. to determine whether the adsorption process results in modifications to the structure of proteins, further work is needed. The heterogeneity of a surface is shown by applying the Freundlich equation Fig.1A (Fahdil A, AL-Niaimi D, 2018). Freundlich isotherms, which are produced by conjugating non-covalent protein-CS/GO -MnO2 NPs, show the various pressures that are exerted on the surfaces of hormone molecules to produce heterogeneity. The initial direction of curvature of the adsorption isotherms Fig.1B (Yano et al., 2022) indicates that as concentration increases, adsorption becomes easier, and more adsorbate is adsorbed upon the first protein monolayer. Stated differently, molecules interact with one another in a side-by-side manner, increasing the adherence of their surfaces. The protein molecule is drawn as far into the aqueous phase as possible by the opposing force of its attraction to water, whereas the adsorption strength is measured as the net of these forces (Singh et al., 2018; Upadhyay et al., 2024). Protein molecules arranged on the surface of the CS/GO-MnO2 NPs according to a variety of factors, and lose their freedom of motion in solution. Changes in conformation can have a significant impact on the protein's adsorption driving force. Identical outcomes have previously been observed (Singh et al., 2018). During adsorption, the protein and hormone interact electrostaticallyCS/GO-MnO2 NPs are negligible. Even exothermic adsorption can occur spontaneously

when the charge of the sorbent and the protein are the same. This complex dependence suggests that the change in enthalpy cannot be explained by a single interaction (Asiri et al., 2020; Tang et al., 2015). Therefore, it is only possible to calculate the ΔH° of the adsorption when sufficient detail about the entire adsorption process is available (Tang et al., 2015). Polar groups' temperature-dependent migration from the protein's inside to its exterior, where they come into contact with water molecules, tends to be exothermic due to the enhanced molecular interactions that result in a negative ΔH° (Fahdil A, AL-Niaimi D, 2018). Such overlap of the repulsion, [MW1] requires that the ΔH for transfer is positive above 25 °C transfer the non- polar group into water [MW2] from the protein's core and negative below 25 0C,[MW3] while the ΔH for transfer from the protein interior into water of the polar group is negative below 25 0C and positive above. [MW4] Hydration entropies of both polar and non-polar groups are negative from about work room temperature (Asiri et al., 2020; Singh et al., 2018; Tang et al., 2015). Seems they both add some structure to the wet land. But these entropies have different dependencies on temperature. Non-polar groups are less able to organize water at higher temperatures and may even contribute to its disorder, as evidenced by the fact that their hydration entropy decreases with temperature (Fahdil A, AL-Niaimi D, 2018). This is because they facilitate the easier rotation of water molecules and have an impact on the size of the hydrogen-bonded network. Because the non-polar groups have more degrees of freedom when the protein unfolds, entropy rises. Because polar groups can create even from more disorganized water, ordered hydration shells, their entropy of hydration is lower and becomes more negative as the temperature rises. As a result, the water becomes more arranged around hydrophilic groups than it would be at higher temperatures, and When hydrophilic hydration occurs, its negative heat capacity increases (Fahdil A, AL-Niaimi D, 2018). The surface of CS/GO-MnO2 NPs spontaneously attaches to hormones due to an electrostatic method of attraction and changes in protein structure (Yano et al., 2022). The relationship between the FSH/LH hormone on the surface of certain NPs has been considered by a number of studies. Our findings are in line with a prior study that determined the primary correlation between the FSH/LH hormones that have the ability to adsorb on nanoparticle surfaces on their own, and indeed additional variables like the adsorption process's thermodynamics, adsorption isotherm, and temperature difference. The findings of this study are consistent with those of Al-Hakeim et al. (Brohi et al., 2017; Fahdil A, AL-Niaimi D, 2018; Wang et al., 2018), who discovered significant differences between the quantity of hormone and the NPs utilized. This work attempts to uncover a significant correlation between the FSH/LH hormone that can spontaneously adsorbed onto the surface of CS/GO-MnO2 NPs. The absorption capacity of FSH and LH hormones by the nanocomposite is quite high (7.07 µg/g of nanocomposite). Freundlich's adsorption isotherm was evaluated in adsorption part suggested that surface of nanocomposite was heterogeneous. [MW1] Thermodynamically, exothermic, spontaneous adsorption mechanisms were observed from the experiments. Another research, the nanocomposites were found to have high of and n values which gave FG of 31.43 and 29.97 mg/g for (FSH) and (LH)[MW2]. A074 of the surface A074 of these hormones of supports our observations (Fahdil A, AL-Niaimi D, 2018). Overall, the results indicated that the composite nanoparticles could efficiently adsorb the LH and FSH molecules, Fig.4 and Table2.

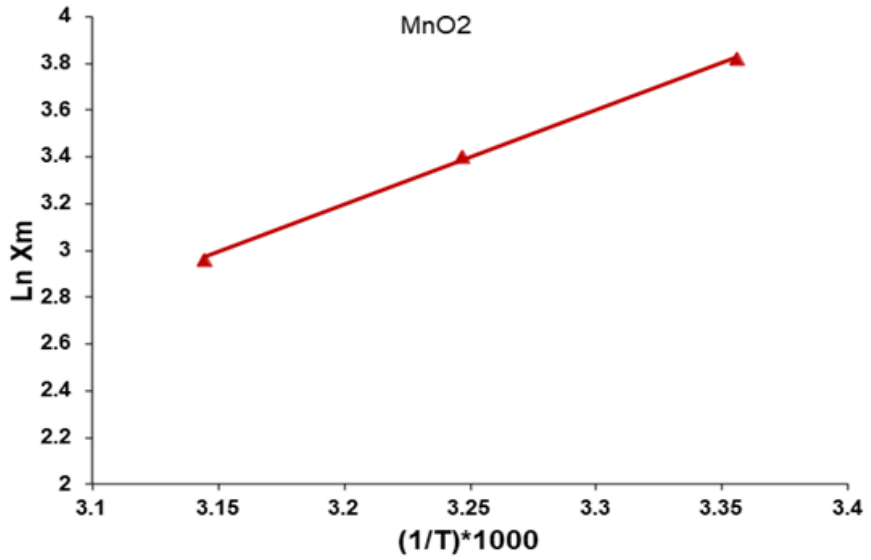

Figure4: Van't Hoff plot for adsorption on MnO_2 nanoparticles showing the relationship between ln K_m and (1/T)×1000. The linear trend indicates the temperature dependence of the adsorption equilibrium constant, allowing estimation of thermodynamic parameters such as ΔH° and ΔS°.

Table2: Thermodynamic Functions (ΔG, ΔH, ΔS) For LH Adsorption On CS/GO-Mno_2 Nanoparticles At 25°C

NPs	(1/T)*1000	Xm=Keq	ln Xm	Slope	ΔG°	ΔH°	ΔS°
CS/GO-MnO_2-NPs	3.356	45.541	3.819	4.073	-9.461	-33.861	-81.880
	3.247	30.051	3.403				
	3.145	19.268	2.958				

3.3 Scanning Electron Microscopy (SEM) of MnO_2-NPs.

The size and shape of the manganese dioxide nanoparticles produced were determined using a scanning electron microscope, as shown in Fig.5. The SEM in Fig.5 illustrates how nearly all of the graphene crystalline nanoparticles on the surface of the MnO2 have nanoscale dimensions. Manganese dioxide (MnO2) displays a range of crystal shapes due to the wide range of corner and/or edge-sharing arrangements of building block units (Jayandran et al., 2015). As seen in Fig.5, the particles in the samples were nearly spherical in form and compactly arranged. SEM images at different magnifications. The size range of the manganese dioxide nanoparticles generated was found to be 28.2 – 40.1 nm.

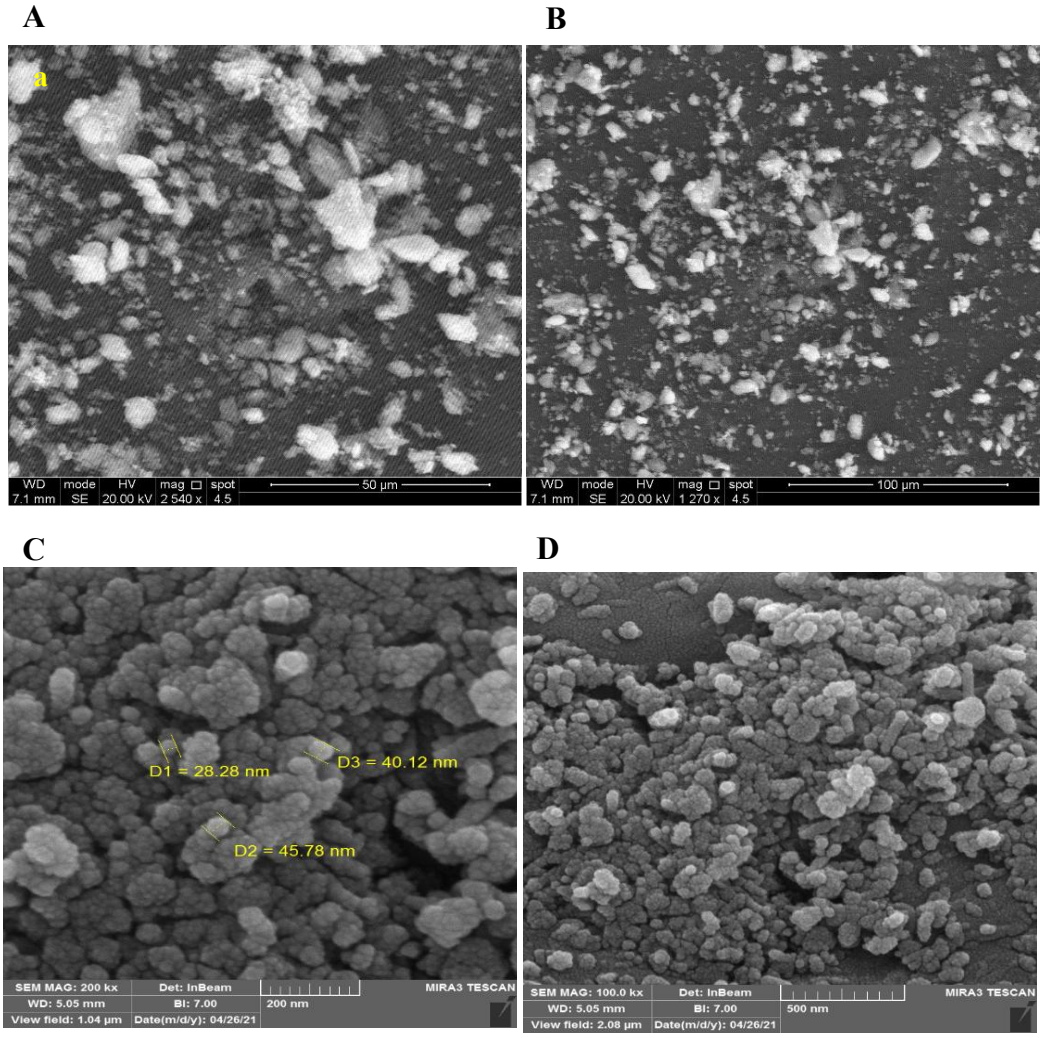

Figure5: Scanning electron microscopy (SEM) images of the synthesized nanoparticles/nanocomposite at different magnifications. The micrographs reveal a heterogeneous and agglomerated surface morphology composed of irregularly shaped particles. Higher magnification images show nanoscale particles with average diameters in the range of approximately 28–46 nm, confirming successful nanoparticle formation and uniform surface coverage, which is favorable for adsorption applications.

3.4 Energy Dispersive X-ray Spectroscopy (EDX) of MnO_2 NPs

The elemental analysis of MnO_2 and CS/GO-MnO_2 NP nanoparticles is displayed in Fig.6. For the structural analysis of the material, energy-dispersive X-ray spectroscopy (EDX) is a suitable analytical technique. The elements Mn and O of the synthetic sample are apparent in Fig.6. It should be noted that the distribution of the atoms was comparable to that of the C, N, O, and Mn atoms in the MnO_2 NPs that were generated. According to EDS data, the proportion of manganese was 7.76%. and the oxygen content was 28.90%, indicating the presence of MnO_2 NPs.

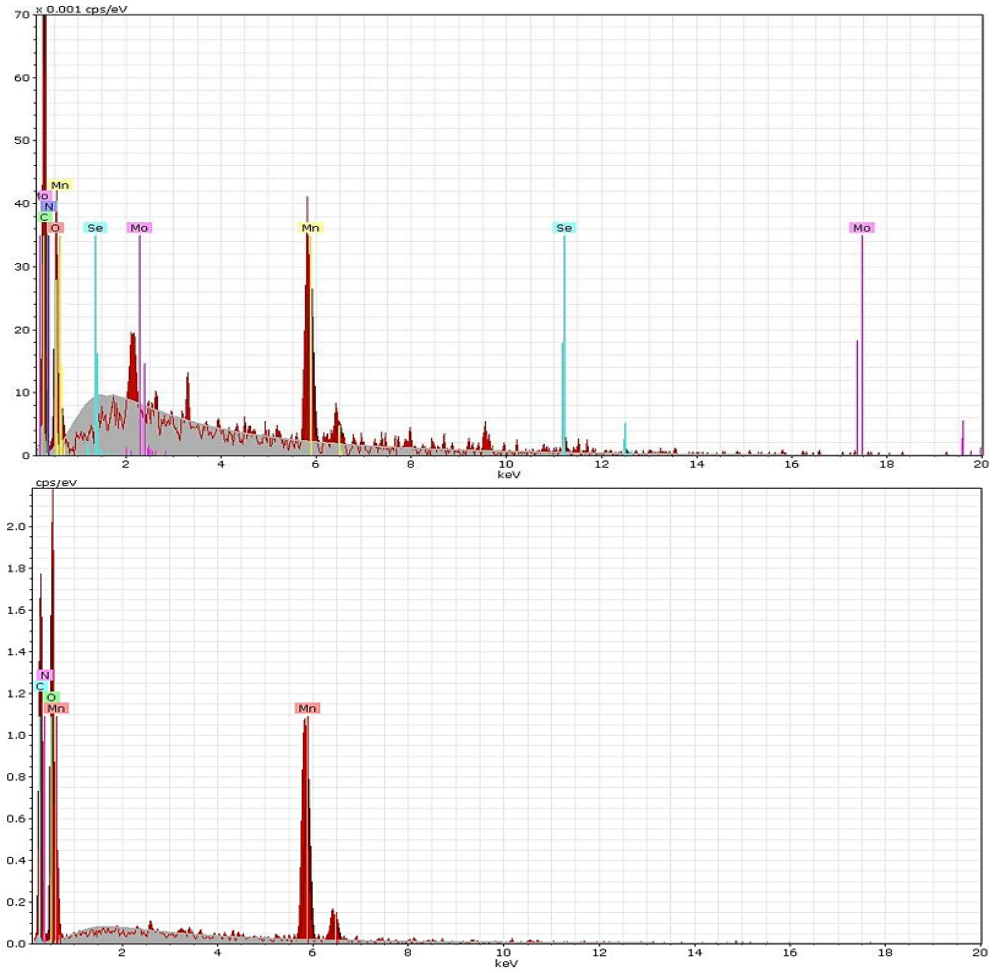

Figure6: Energy-dispersive X-ray spectroscopy (EDS) spectra of the synthesized nanoparticles/nanocomposite. The spectra confirm the presence of manganese (Mn) and oxygen (O) as the main constituents, along with carbon (C) and nitrogen (N) originating from chitosan and graphene oxide. The absence of significant impurity peaks indicates high purity and successful synthesis of the MnO_2-based nanomaterial.

3.5 X-Ray Diffraction (XRD) of MnO_2 NPs

XRD was used to investigate the crystal structure of MnO2 NP nanocomposites spanning the 2θ angle range from 10o to 80o. The produced powder's XRD pattern is illustrated in Fig.7. The manganese dioxide particles were subjected to X-ray technology analysis utilizing an X-ray diffractometer. Fig.8 displays the XRD patterns for powdered MnO2 NPs. The quantity of peaks found in these nanoparticles at 370 angles is caused by the massive generation of crystalline manganese dioxide nanoparticles. Many polymorphs, or distinct crystal structures, of MnO2 are known to exist, including the α-, β-, γ-, δ-, ε-, and λ-types, among others. The arrangement of the [MnO6] octahedron's basic structural unit separates each polymorph from the others. These octahedral linkages indicate that MnO2 can exist as a 3D structure such as the λ-type, as a layered or sheet structure such as δ-MnO2, or as a tunnel structure resembling a chain, such as the α-, β-, and γ-types. Phases H2O2-, H2O2-, and H2O2- have one-dimensional (1D) tunnels with X*X octahedral cross sections (X = 1, 2, 3, or 4); phase H2O2- is a two-dimensional compound, while phase H2O2- has a three-dimensional spinel structure (Andris et al., 2021; Shaker & AbdAlsalm, 2018; Smith et al., 2016). The MnO2 NPs identified by Debye-Scherer had an average size

of about 28.2 nm, based on the results of the XRD pattern examinations. The existence of 37.1, the phase's highest peak, suggests that the -MnO2 phase is the dominant phase according to the standard (JCPDS: 44 - 0141) (Andris et al., 2021; Jayandran et al., 2015; Shaker & AbdAlsalm, 2018; Smith et al., 2016).

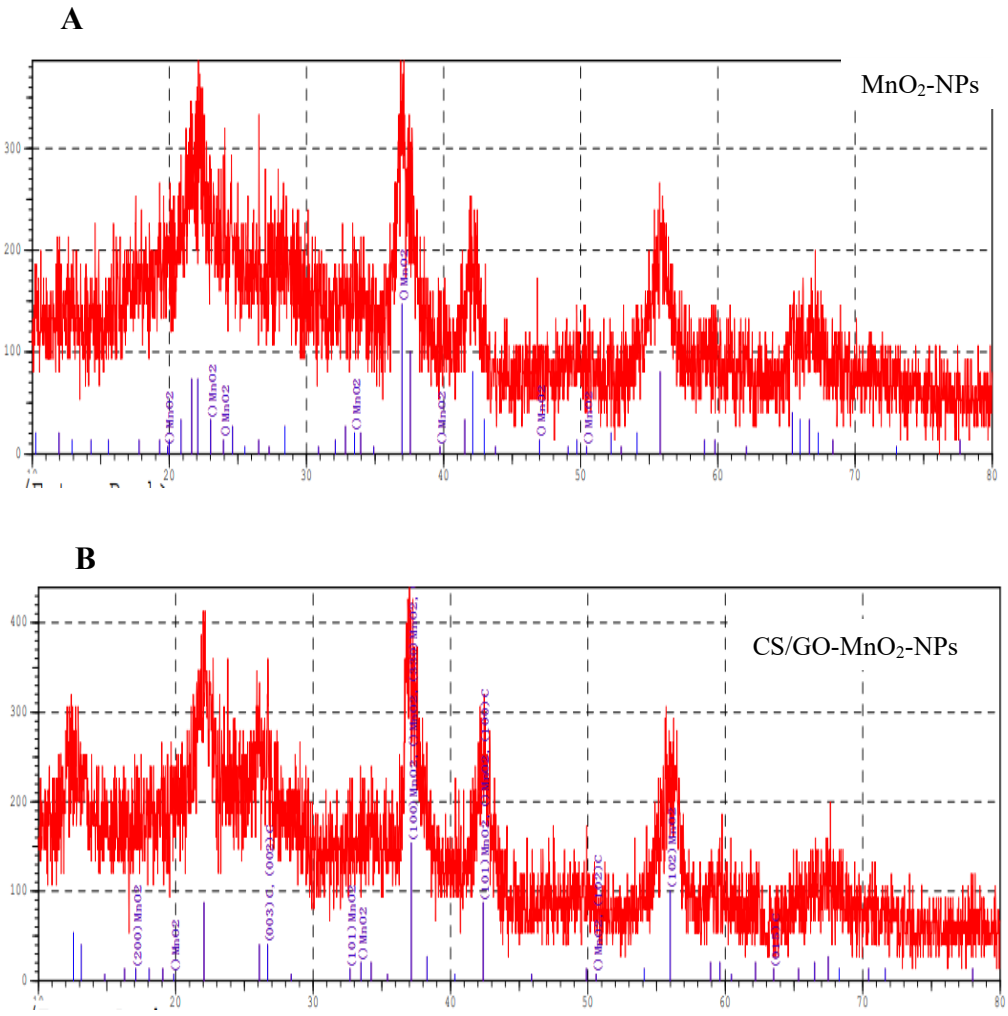

Figure7: X-ray diffraction (XRD) patterns of (A) MnO_2 nanoparticles (MnO_2-NPs) and (B) chitosan/graphene oxide–MnO_2 nanocomposites (CS/GO-MnO_2-NPs). The characteristic diffraction peaks confirm the crystalline structure of MnO_2, while peak broadening and intensity variations in the nanocomposite indicate successful incorporation of chitosan and graphene oxide without altering the MnO_2 crystal phase.

3.6 Fourier Transform Infrared Spectrophotometer (FTIR) of MnO_2-NPs.

The type and purity of manganese dioxide metal nanoparticles generated by the co-precipitation technique were determined using FTIR spectroscopy, as shown in Fig.8. The quality and makeup of manganese dioxide metal nanoparticles made by the co-precipitation technique were evaluated using FTIR spectroscopy. This method relies heavily on highly precise and sensitive interference. The functional groups found in the generated manganese dioxide nanoparticles are shown in Fig.8. The two absorption bands at 588.31– 842.94 cm-1 are related to the stretching vibration of O–Mn–O, suggesting

the presence of MnO2, although the bands in the 400–800 cm-1 range are assumed to be Mn-O vibrations. The presence of O-H, C=O, C-C, Mn-C, Mn-O, and Mn can be inferred from the peaks at 2969, 1442, 1377, 1037, and 842 cm-1. The broad absorption bands in the 4000–3000 cm-1 region is ascribed to both hydroxyl group and H–O–H stretching vibrations [1]. The bending vibration of an adsorbed water molecule was identified as the cause of the peak at 1770 cm-1.

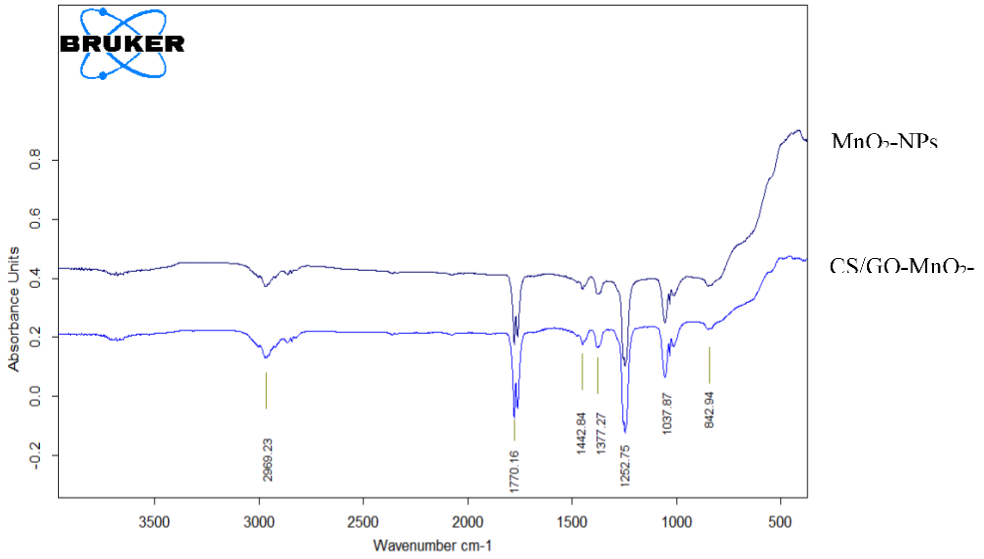

Figure8: Fourier-transform infrared (FTIR) spectra of MnO_2 nanoparticles (MnO_2-NPs) and chitosan/graphene oxide–MnO_2 nanocomposites (CS/GO-MnO_2-NPs). The spectra show characteristic absorption bands corresponding to Mn–O vibrations, as well as functional groups associated with chitosan and graphene oxide, confirming successful surface modification and formation of the nanocomposite.

3.7 Particle Size Distribution of MnO_2 NPs

The measurement of the particle size distribution of the CS/GO-MnO2 NP nanocomposite and MnO2 NPs is displayed in Fig.9. According to the size distribution histogram obtained from DLS, the size range of these MnO2 particles is 561–566 nm. Version 7.01 of the Malvern Zetasizer Particle Size Analyzer Software was used to verify the measurement of the particle size distribution. The size particle distribution of MnO2 NPs was suggested by the strong peak observed in Fig.9 at 28.2 nm. The addition of chitosan and graphene oxide causes the nanoparticles to agglomerate less while increasing in size. Graphene and chitosan have a narrower particle size distribution than manganese dioxide. The additives prevent manganese oxide nanoparticles from aggregating by influencing particle size and size distribution as a result of their adsorption onto the surface of MnO2 nanoparticles. Consequently, graphene oxide would be the surface additive that is most strongly adsorbed (“Malvern Instruments Inc.,” 1986; Rahman et al., 2021; Rinaudo, 2006).

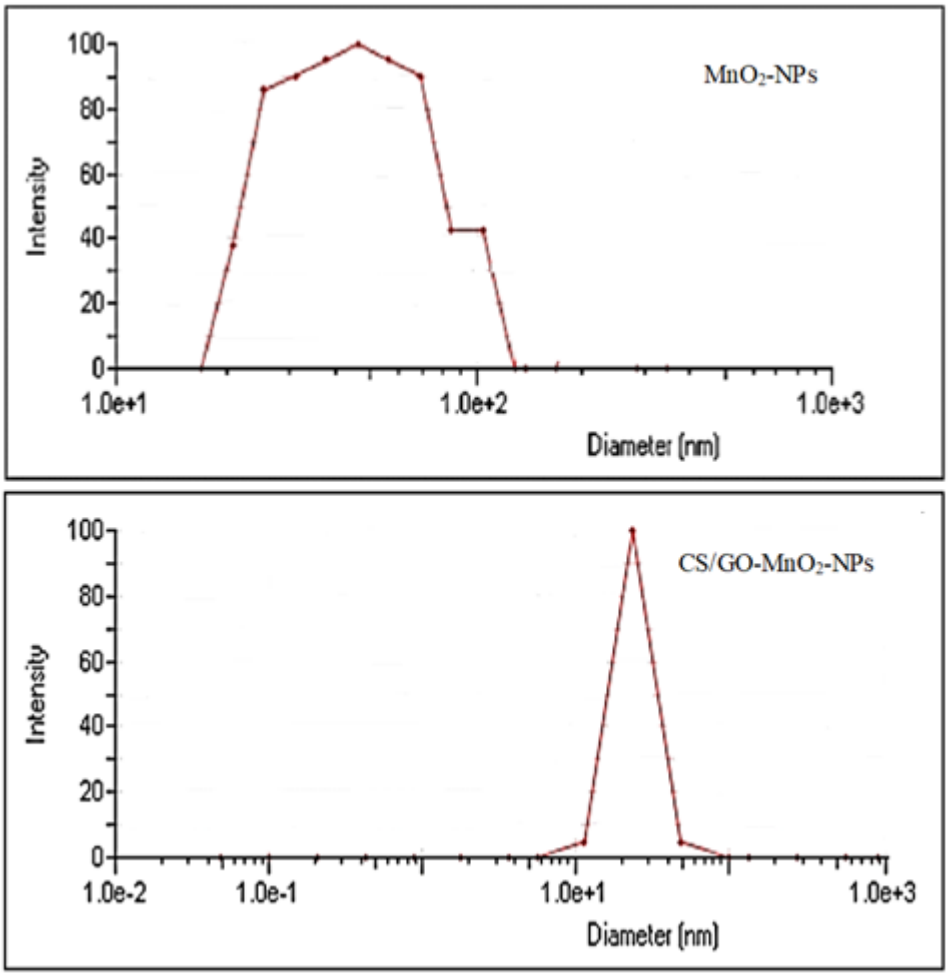

Figure9: Dynamic light scattering (DLS) size distribution of MnO_2 nanoparticles (MnO_2-NPs) and chitosan/graphene oxide–MnO_2 nanocomposites (CS/GO-MnO_2-NPs). The results show a narrower and more uniform particle size distribution for the CS/GO-MnO_2-NPs compared with MnO_2-NPs, indicating improved dispersion and stability after surface modification.

3.8 Zeta Potential Analysis of MnO_2 NPs

Fig.10 shows the MnO2 NPs dispersion zeta potentials as a function of pH. A charge on a particle's surface results in a zeta potential, which can have either a positive or negative polarity depending on the chemistry of the particle. The level of repulsion between particles in a formulation that have similar charges is measured by the zeta potential. Repulsive forces prevent particles from clumping while being stored. Thus, a formulation's zeta potential indicates the likelihood of its physical stability. Fig.10 shows how the zeta potential changes. Additionally, particle size. The zeta potential ranged from -19.67 mV to -20.73 mV, with the latter seemingly dependent on pH. TThe pH was 7.3. As pH drops, the zeta potential rises. The dispersion of MnO2 NPs' zeta potential as a function of pH is shown in Fig.10, and is constant for all production procedures. The zeta potential is positive when the pH is less than 5.5 and negative when the pH is increased to about pH = 5.6. The zeta-potential is determined by the interaction of

nanoparticles with water ions [1]. The Helmholtz-Smoluchowski equation, $\zeta = E\ (4\pi\eta\ /\varepsilon)$, was utilized to convert the electrophoretic mobility to a zeta potential. In this equation, ζ is the zeta potential (mV), E is the electrophoretic mobility, η is the viscosity of the dispersion medium, and ε is the solvent's dielectric constant (Hou et al., 2022; Tadros, 1982; Vold, 1982; Zhang et al., 2019).

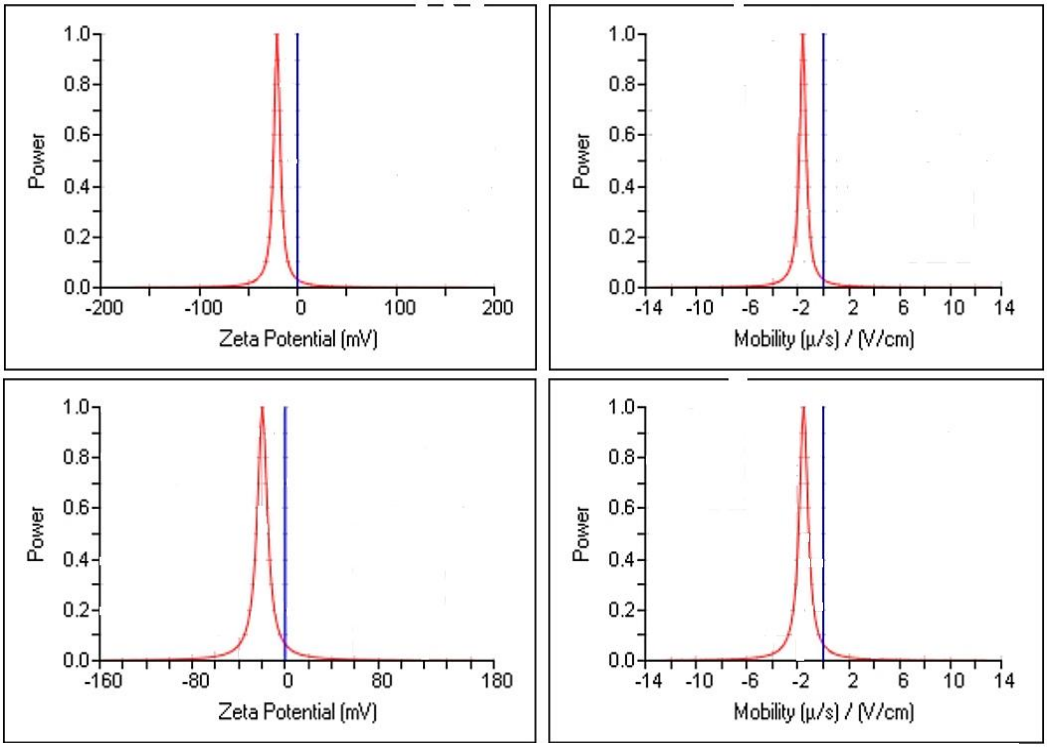

Figure10: Zeta potential and electrophoretic mobility distributions of MnO_2 nanoparticles (MnO_2-NPs) and chitosan/graphene oxide–MnO_2 nanocomposites (CS/GO-MnO_2-NPs) The surface modification results in a shift in zeta potential, indicating enhanced surface charge and improved colloidal stability of the nanocomposite.

4.Conclusion

The findings of our study reveal the success of the chemical method for MnO2 NP production, fabricated in flakes. Chitosan, a biopolymer, has been used to chemically synthesize a MnO2 NP composite. Conclusions The study demonstrates the immense scope that chitosan-coated MnO_2 nanoparticles could have in biomedical applications. These nanoparticles adsorb FSH and LH hormones in human serum effectively as a composite with organic molecules.

References

Andris, R., Ridley, P., Byles, B. W., Cullen, D. A., More, K. L., & Pomerantseva, E. (2021). Synthesis strategies toward improved ordering of [MnO6] octahedra in tunnel structured 2 × 3 and 2 × 4 MnO2. *Scripta Materialia*, *195*. https://doi.org/10.1016/j.scriptamat.2020.113713

Asiri, S. M. M., Cevik, E., Sabit, H., & Bozkurt, A. (2020). Alginate-guided size and morphology-controlled synthesis of MnO2 nanoflakes. *Soft Materials*, *18*(1). https://doi.org/10.1080/1539445X.2019.1672192

Brohi, R. D., Wang, L., Talpur, H. S., Wu, D., Khan, F. A., Bhattarai, D., Rehman, Z. U., Farmanullah, F., & Huo, L. J. (2017). Toxicity of nanoparticles on the reproductive system in animal models: A review. In *Frontiers in Pharmacology* (Vol. 8, Issue SEP). https://doi.org/10.3389/fphar.2017.00606

Fahdil A, AL-Niaimi D, O. A. (2018). Adsorption of Orange G Dye from Aqueous Solutions Using Magnesium Oxide Nanoparticles. *Journal of Biochemical Technology*, *9*(3).

Hou, X., Li, J., Li, Y., & Tian, Y. (2022). Intermolecular and surface forces in atomic-scale manufacturing. *International Journal of Extreme Manufacturing*, *4*(2). https://doi.org/10.1088/2631-7990/ac5e13

Jayandran, M., Muhamed Haneefa, M., & Balasubramanian, V. (2015). Green synthesis and characterization of Manganese nanoparticles using natural plant extracts and its evaluation of antimicrobial activity. *Journal of Applied Pharmaceutical Science*, *5*(12). https://doi.org/10.7324/JAPS.2015.501218

Malvern Instruments Inc. (1986). *Analytical Chemistry*, *58*(7). https://doi.org/10.1021/ac00298a766

Nugroho, T., Prajoko, B., & Suryawan, I. G. S. (2023). Analysis of Clay Mineral Transformation in Plambik Village, Central Lombok Using X-Ray Diffraction and Scanning Electron Microscope Methods. *Journal of Physics and Its Applications*, *6*(1). https://doi.org/10.14710/jpa.v6i1.19011

Petrov, A. I., Volodkin, D. V., & Sukhorukov, G. B. (2005). Protein-calcium carbonate coprecipitation: A tool for protein encapsulation. *Biotechnology Progress*, *21*(3). https://doi.org/10.1021/bp0495825

Rahman, M. H., Werth, H., Goldman, A., Hida, Y., Diesner, C., Lane, L., & Menezes, P. L. (2021). Recent progress on electroactive polymers: Synthesis, properties and applications. In *Ceramics* (Vol. 4, Issue 3). https://doi.org/10.3390/ceramics4030038

Rinaudo, M. (2006). Chitin and chitosan: Properties and applications. Progress in Polymer. *Progress in Polymer Science, 31*(7).

Shaker, K., & AbdAlsalm, A. (2018). Synthesis and Characterization Nano Structure of MnO2 via Chemical Method. *Engineering and Technology Journal*, *36*(9A). https://doi.org/10.30684/etj.36.9a.1

Singh, T., Sharma, R. K., & Singh, G. (2018). MnO2 Nanoparticles Embedded Polypyrrole Nanotubes for Supercapacitor Electrodes. In *Green Chemistry in Environmental Sustainability and Chemical Education*. https://doi.org/10.1007/978-981-10-8390-7_19

Smith, P. F., Deibert, B. J., Kaushik, S., Gardner, G., Hwang, S., Wang, H., Al-Sharab, J. F., Garfunkel, E., Fabris, L., Li, J., & Dismukes, G. C. (2016). Coordination Geometry and Oxidation State Requirements of Corner-Sharing MnO6 Octahedra for Water Oxidation Catalysis: An Investigation of Manganite (γ-MnOOH). *ACS Catalysis*, *6*(3). https://doi.org/10.1021/acscatal.6b00099

Tadros, TharwatF. (1982). Zeta potential in colloid science. Principles and application. *Colloids and Surfaces*, *5*(1). https://doi.org/10.1016/0166-6622(82)80060-7

Tang, Y., Chen, T., & Yu, S. (2015). Morphology controlled synthesis of monodispersed manganese sulfide nanocrystals and their primary application in supercapacitors with high performances. *Chemical Communications*, *51*(43). https://doi.org/10.1039/c5cc01700a

Upadhyay, J., Borah, R., Das, T. M., & Das, J. M. (2024). Fabrication of flexible supercapacitor of Polypyrrole nanotubes embedded with Ruthenium oxide nanoparticles for enhanced electrochemical performance. *Electrochimica Acta*, *503*. https://doi.org/10.1016/j.electacta.2024.144858

Vold, M. J. (1982). Zeta potential in colloid science. Principles and applications. *Journal of Colloid and Interface Science*, *88*(2). https://doi.org/10.1016/0021-9797(82)90296-x

Wang, R., Song, B., Wu, J., Zhang, Y., Chen, A., & Shao, L. (2018). Potential adverse effects of nanoparticles on the reproductive system. In *International Journal of Nanomedicine* (Vol. 13). https://doi.org/10.2147/IJN.S170723

Yano, H., Aimi, A., Sakai, N., Sasaki, T., & Fujimoto, K. (2022). Single-Crystal Growth of Layered Birnessite-Type Manganese Oxides and Their Delamination into MnO2 Nanosheets. *Crystal Growth and Design*, *22*(1). https://doi.org/10.1021/acs.cgd.1c01171

Zhang, L., Xie, L., Cui, X., Chen, J., & Zeng, H. (2019). Intermolecular and surface forces at solid/oil/water/gas interfaces in petroleum production. *Journal of Colloid and Interface Science*, *537*. https://doi.org/10.1016/j.jcis.2018.11.052